Title

High-Performance Oligomeric Catholytes for Effective Macromolecular Separation in Nonaqueous Redox Flow Batteries

Journal

ACS Central Science, 4(2)

ISSN

2374-7943

Authors

Hendriks, Koen H

Robinson, Sophia G

Braten, Miles N

et al.

Publication Date

2018-02-28

DOI

10.1021/acscentsci.7b00544

Peer reviewed

ACS central science

Research Article

Cite This: ACS Cent. Sci. 2018, 4, 189−196

High-Performance Oligomeric Catholytes for Effective Macromolecular Separation in Nonaqueous Redox Flow Batteries

Koen H. Hendriks,[†,‡] Sophia G. Robinson,[‡,§] Miles N. Braten,[‡,∥] Christo S. Sevov,[†,‡] Brett A. Helms,[‡,∥] Matthew S. Sigman,[‡,§] Shelley D. Minteer,[‡,§] and Melanie S. Sanford*[,†,‡]

[†]Department of Chemistry, University of Michigan, 930 North University Avenue, Ann Arbor, Michigan 48109, United States
[§]Department of Chemistry, University of Utah, 315 South 1400 East, Salt Lake City, Utah 84112, United States
[∥]The Molecular Foundry, Lawrence Berkeley National Laboratory, 1 Cyclotron Road, Berkeley, California 94720, United States
[‡]Joint Center for Energy Storage Research (JCESR), 9700 S. Cass Avenue, Argonne, Illinois 60439, United States

Supporting Information

ABSTRACT: Nonaqueous redox flow batteries (NRFBs) represent an attractive technology for energy storage from intermittent renewable sources. In these batteries, electrical energy is stored in and extracted from electrolyte solutions of redox-active molecules (termed catholytes and anolytes) that are passed through an electrochemical flow cell. To avoid battery self-discharge, the anolyte and catholyte solutions must be separated by a membrane in the flow cell. This membrane prevents crossover of the redox active molecules, while simultaneously allowing facile transport of charge-balancing ions. A key unmet challenge for the field is the design of redox-active molecule/membrane pairs that enable effective electrolyte separation while maintaining optimal battery properties. Herein, we demonstrate the development of oligomeric catholytes based on tris(dialkylamino)cyclopropenium (CP) salts that are specifically tailored for pairing with size-exclusion membranes composed of polymers of intrinsic microporosity (PIMs). Systematic studies were conducted to evaluate the impact of oligomer size/structure on properties that are crucial for flow battery performance, including cycling stability, charge capacity, solubility, electron transfer kinetics, and crossover rates. These studies have led to the identification of a CP-derived tetramer in which these properties are all comparable, or significantly improved, relative to the monomeric counterpart. Finally, a proof-of-concept flow battery is demonstrated by pairing this tetrameric catholyte with a PIM membrane. After 6 days of cycling, no crossover is detected, demonstrating the promise of this approach. These studies provide a template for the future design of other redox-active oligomers for this application.

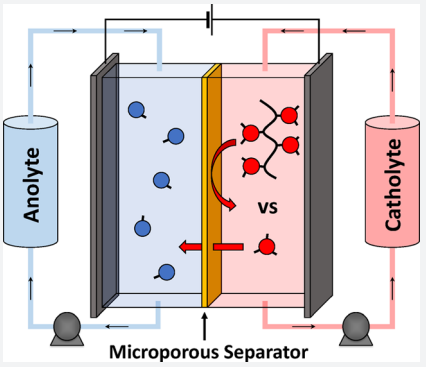

INTRODUCTION

Nonaqueous redox flow batteries (NRFBs) are a promising electrical energy storage technology for the integration of intermittent renewable energy sources into the electrical grid.[1−5] NRFBs store energy in soluble redox-active molecules—anolytes and catholytes—that are stored in external tanks separate from the electrodes.[6,7] This configuration permits the independent scaling of energy capacity and power, which is not possible with more traditional solid state batteries (e.g., Li ion batteries).[8−10] In recent years, aqueous redox flow batteries have been extensively explored and shown to exhibit stable cycling and good energy densities.[11−14] The substitution of water with a nonaqueous solvent (e.g., acetonitrile or propylene carbonate) would enable theoretical cell voltages as high as ∼5 V, which represents an approximately 4-fold increase over established aqueous RFB technologies.[15] Toward this end, there has been significant effort directed at the development of organic molecules that meet many of the criteria necessary for application in NRFBs (e.g., large potential window, high stability, high solubility).[16−20] Despite this progress, a key challenge remains for the deployment of these promising materials in full flow batteries. Specifically, there are limited types of membranes that are suitable for testing state-of-the-art organic anolyte/catholyte pairs in unsymmetrical nonaqueous flow batteries.[21,22]

The membrane serves two crucial, and often opposing, roles in a flow battery. First, it must facilitate passive transport of the supporting electrolyte ions in order to maintain charge neutrality during battery operation. Simultaneously, the membrane must prevent transport of the anolyte and catholyte molecules between the two compartments of the NRFB (Figure 1), since crossover of the redox-active species results in low Coulombic efficiency and irreversible loss of battery capacity. This problem has been addressed in the area of aqueous RFBs through the use of ion exchange membranes that possess an ionic bias to exclude redox-active molecules of a specific charge.[15] However, these membranes are typically incompatible with nonaqueous solvents, as these solvents lead

Received: November 9, 2017
Published: January 17, 2018

DOI: 10.1021/acscentsci.7b00544
ACS Cent. Sci. 2018, 4, 189−196

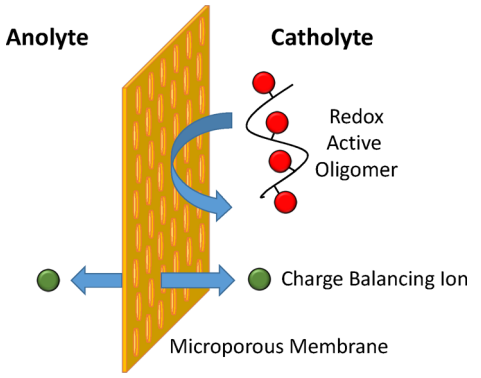

Figure 1. Schematic representation of the operation of a microporous membrane in a flow battery using redox-active oligomers.

to mechanical and chemical failures that compromise the membrane's ability to prevent crossover.[21,22]

A promising strategy is the use of size-exclusion membranes that are compatible with nonaqueous solvents. In principle, such membranes could enable the rapid diffusion of small charge-balancing ions, while precluding the crossover of redox-active molecules that exceed the dimensions of the membrane's pores. This concept has recently been demonstrated by pairing mesoporous membranes with polymer-supported redox-active molecules in both aqueous[23] and nonaqueous media.[24−27] However, the tethering of redox-active molecules to high molecular weight polymers introduces a new set of fundamental challenges.[24] First, the close proximity of redox-active centers often leads to reduced electrochemical stability.[28] Additionally, the polymer solutions are often plagued by adsorption of active species onto the electrodes, slow diffusion rates, and high viscosities, all of which impede effective flow battery operation.[24,27] Overall, these studies demonstrate that solutions to the membrane problem will likely require careful consideration/redesign of the redox-active anolyte or catholyte materials.

Our approach to addressing these challenges involves the design of redox-active oligomers (RAOs) that can be paired with microporous membranes in nonaqueous media. We hypothesized that RAOs can be tailored to display physical properties more similar to those of monomeric redox-active molecules than to polymers, while still allowing for separation by size exclusion. A recent report by Helms demonstrated that membranes composed of polymers of intrinsic microporosity (PIMs) are effective at slowing the crossover of viologen, pyridinium, and alkoxyarene oligomers in organic solvents, while maintaining high conductivity of the working ion.[29,30] In particular, trimeric viologen and pyridinium derivatives were completely excluded from crossover over 450 h under the tested conditions. This is an exciting demonstration of the size-exclusion principle. However, implementation of this concept in a full flow battery has not been demonstrated, as it hinges on the identification of RAOs that minimize the aforementioned liabilities associated with redox-active polymers.

This article describes our systematic studies aimed at the identification of RAOs that maintain favorable physical properties compared to their monomeric counterparts.[28] Tris(dialkylamino)cyclopropenium (CP) catholytes were selected as a test case for this study based on our recent report describing the monomeric analogue as a high potential, stable catholyte for NRFBs.[19] Because the CP monomer has been well-characterized, the development of CP oligomers affords the opportunity for direct comparison of the physical attributes of the oligomers with the parent monomer. We demonstrate herein that the evaluation of a library of CP oligomers led to the identification of a derivative whose stability, charge capacity, electron transfer kinetics, and crossover rates are all comparable to, or significantly improved relative to, the monomeric counterpart. The optimal RAO (a CP-tetramer) was combined with a PIM-1/Celgard membrane stack in a proof-of-concept flow battery, which, over 6 days of cycling, resulted in no detectable crossover of the RAO. These studies provide the first detailed template for the design of RAOs for this application.

RESULTS AND DISCUSSION

As described above, our overall objective was to transform a recently reported high potential catholyte, a tris(dialkylamino)-cyclopropenium (CP) salt, into oligomeric variants to be paired with a PIM-1 membrane. In order to do this, we sought to quantitatively assess the impact of oligomer structure on key metrics for flow battery materials, including redox potential, stability, diffusion, electron transfer kinetics, and crossover. In order to rapidly evaluate all of these parameters, we first needed a modular synthetic approach for accessing a library of CP oligomers. As shown in Scheme 1, our synthetic approach

Scheme 1. Synthesis and Chemical Structures of Cyclopropenium-Based Oligomers

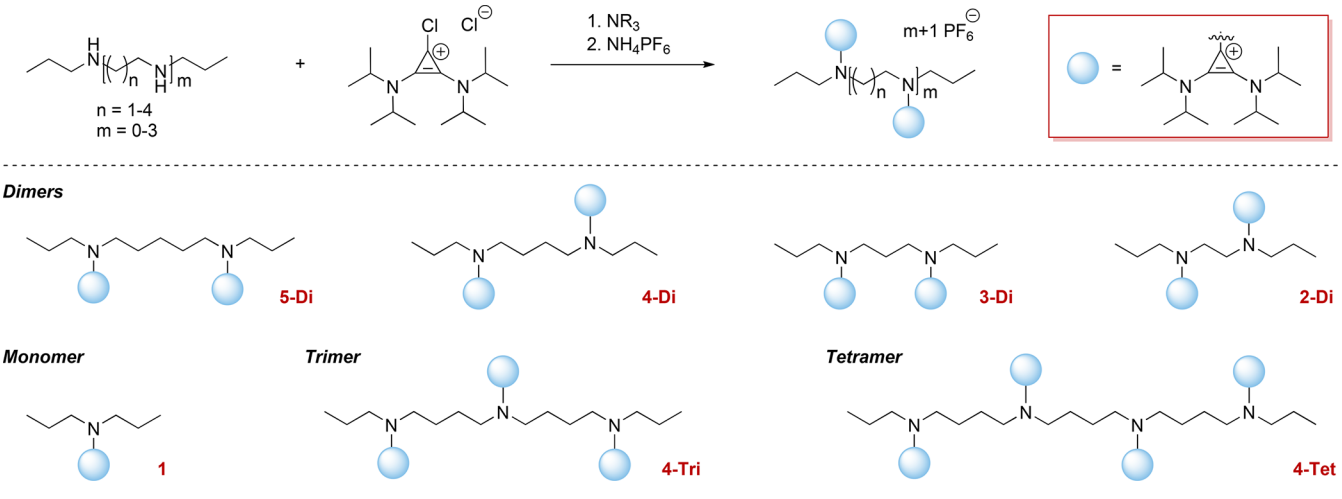

DOI: 10.1021/acscentsci.7b00544
ACS Cent. Sci. 2018, 4, 189−196

leverages readily available chlorobis(dialkylamino)-cyclopropenium as a key building block. The reaction of this precursor with different mono-, di-, tri-, and tetraamine starting reagents yields the corresponding monomeric, dimeric, trimeric, and tetrameric CP derivatives in 59−98% yield (see Supporting Information for complete details of synthesis and purification).

We first prepared a series of CP dimers in which the distance between the redox-active CP moieties is varied from two to five carbons (Scheme 1, **2-Di**−**5-Di**). This series allowed us to systematically evaluate the impact of linker length on the electrochemical potential and stability of these molecules using cyclic voltammetry and galvanostatic bulk electrolysis (Figure 2). Overall, this series shows that a linker of at least four

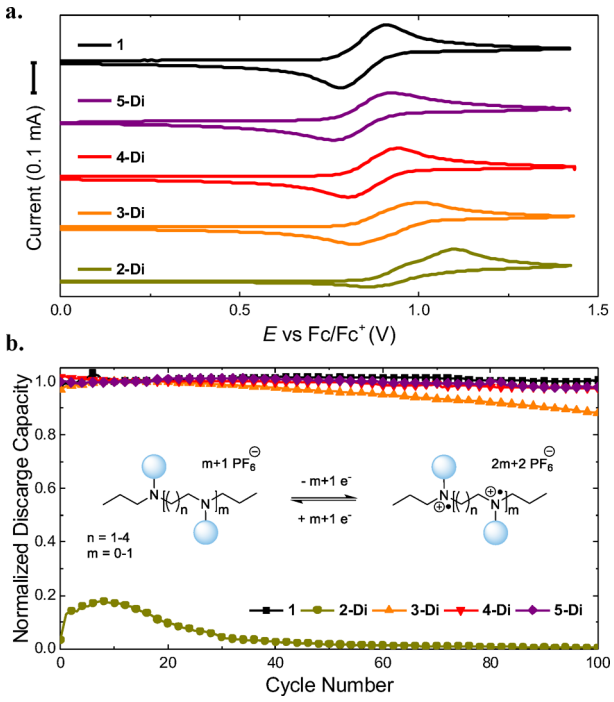

Figure 2. (a) Cyclic voltammograms of **1** (6 mM) and **2-Di**−**5-Di** (3 mM) at a glassy carbon working electrode, platinum wire auxiliary electrode, and Ag/Ag^+ reference electrode at a 100 mV s^{-1} scan rate. (b) Charge/discharge cycling data for H-cell bulk electrolysis of the same solutions using RVC electrodes (~70 cm^2 surface area) with 5 mA current and voltaic cutoffs of 1.2−1.3 V vs Ag/Ag^+ (~1.15 V−1.25 V vs Fc/Fc^+). The inset shows the multielectron redox reaction of the CP dimer series during cycling. Both sets of experiments were performed in acetonitrile with 0.5 M $LiPF_6$ supporting electrolyte.

carbons is required in order for the oligomer to exhibit both electrochemical and stability properties that are analogous to those of the corresponding monomer. For example, the ethyl-linked dimer **2-Di** exhibits two distinct oxidation peaks in its cyclic voltammogram, corresponding to successive oxidation of the two CP units. A single reduction peak is observed on the return sweep (Figure 2a). These features indicate that, with this short linker, the two CP units are electronically coupled. The *n*-propyl-linked dimer **3-Di** shows a broad oxidation peak (peak width, $E_p - E_{p/2}$ = 0.17 V) and a quasi-reversible reduction peak, suggesting that significant electronic interactions between the CP units persist with the *n*-propyl linker. In contrast, the CVs of **4-Di** and **5-Di** show single, quasi-reversible oxidation and reduction waves that are nearly identical to those of the monomer **1** ($E_{1/2}$ = 0.87 V vs Fc/Fc^+, $E_p - E_{p/2}$ = 0.09 V).

For application in NRFBs, it is imperative that the catholyte be electrochemically stable for thousands of charging and discharging cycles. To simulate this process, 3 mM dimer solutions were subjected to bulk electrolysis charge/discharge cycling in an H-cell.[31,32] The solutions were charged and discharged for 100 cycles at 5 mA (~5 C rate) using voltaic limits to reach maximum achievable state-of-charge (SOC). As shown in Figure 2b, the dimer **2-Di** exhibited extremely poor cycling stability, with >80% capacity fade observed after a single cycle.[33] Extension of the linker by one carbon to **3-Di** coincided with a significant improvement in cycling stability, with ~12% capacity fade over 100 cycles. Furthermore, dimers **4-Di** and **5-Di** displayed extremely high cycling stability that is comparable to that of monomer **1**, with <5% fade over 100 cycles, reaching an average 94% state-of-charge. In summary, these initial electrochemical studies demonstrate a requirement for a minimum 4-carbon spacer to isolate the redox chemistry of the CP units and thus provide electrochemical performance comparable to that of the monomer.

The promising electrochemical properties of dimers **4-Di** motivated the examination of analogous oligomers possessing more CP units, as a larger size is expected to enhance their desired exclusion by PIM-1 membranes (Scheme 1).[29] Accordingly, the trimer (**4-Tri**) and tetramer (**4-Tet**) analogues bearing an *n*-butyl linker between the CP moieties were synthesized (Scheme 1). The electrochemical stability of these species was evaluated using the same procedures as for the dimer series. As depicted in Figure 3a, the CVs of **1**, **4-Di**, **4-Tri**, and **4-Tet** exhibit nearly identical standard redox potentials and peak widths ($E_{1/2}$ = +0.86 V vs Fc/Fc^+, $E_p - E_{p/2}$ = 0.09 V). Bulk electrolysis of these species in an H-cell for 100 charge/discharge cycles revealed that a high state-of-charge (93−98%) can be achieved independent of oligomer size. This is particularly remarkable considering that the 98% state of charge of **4-Tet** indicates the formation of the octacationic tetraradical species **4-Tet**$^{4+}$ (Figure 3b). Furthermore, all of these oligomers exhibit excellent stability profiles, with <5% fade of the discharge capacity over 100 cycles (see Figure 3b and Figure S3 for cycling data).

Mass transfer and electrokinetics are important processes for NRFB application.[34] In order to access high current densities and minimize overpotentials, it is essential that the RAOs display fast diffusional and electron-transfer processes. Particularly in the case of oligomers, this includes self-exchange reactions between oxidized and reduced redox sites along the chain that enable rapid access to all redox centers.[24] To evaluate the effect of oligomerization on diffusional processes, the diffusion coefficients for **1**, **4-Di**, **4-Tri**, and **4-Tet** and their electrochemically oxidized analogues **1**$^+$, **4-Di**$^{2+}$, **4-Tri**$^{3+}$, and **4-Tet**$^{4+}$ were determined via cyclic voltammetry. As predicted by the Stokes−Einstein relation, the diffusion coefficients of these molecules decrease with increasing molecular weight (Table 1). Comparison of **1**, **4-Di**, **4-Tri**, and **4-Tet** reveals that the diffusion coefficients diminish by roughly 50% with the addition of each successive CP unit, decreasing from 7.0 ± 0.2 × 10^{-6} cm^2 s^{-1} for monomer **1** to 5.3 ± 0.2 × 10^{-7} cm^2 s^{-1} for tetramer **4-Tet**. A similar trend is observed for the oxidized forms of these catholytes, **1**$^+$, **4-Di**$^+$, **4-Tri**$^+$, and **4-Tet**$^+$. For the oxidized species, the values are all ~2-fold lower than those of the nonoxidized analogues, likely due to the higher overall charge of the oxidized molecules (Table 1). Overall, these data

DOI: 10.1021/acscentsci.7b00544
ACS Cent. Sci. 2018, 4, 189−196

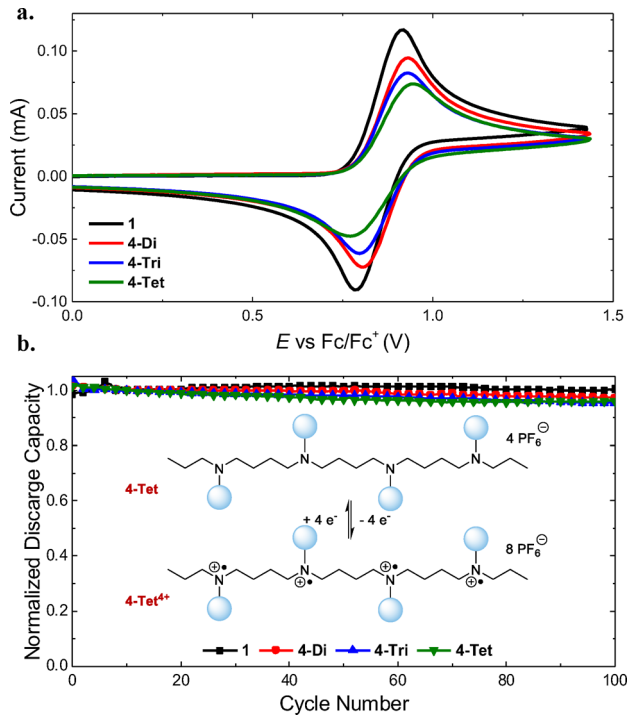

Figure 3. (a) Cyclic voltammograms of monomer **1** (6 mM), **4-Di** dimer (3 mM), **4-Tri** trimer (2 mM), and **4-Tet** tetramer (1.5 mM) at a glassy carbon working electrode, platinum wire auxiliary electrode, and Ag/Ag^+reference electrode at a 100 mV s^{-1}scan rate. (b) Bulk electrolysis performed in H-cell of the same solutions using RVC electrodes and 5 mA current with voltaic cutoff of 1.2 V vs Ag/Ag^+ (~1.15 V vs Fc/Fc^+). The inset shows the overall redox reaction for **4-Tet**. Both sets of experiments were performed in acetonitrile with 0.5 M $LiPF_6$ supporting electrolyte.

demonstrate that oligomerization results in a small penalty in diffusion rate. It is important to note that diffusion coefficients on the order of 10^{-7} cm^2 s^{-1} are still appropriate for flow battery applications.[17]

To probe the impact of oligomer size on the electron-transfer kinetics, heterogeneous electron-transfer rates (k_0) between a glassy carbon working electrode and the solution were determined using the Nicholson method for **1**, **4-Di**, **4-Tri**, and **4-Tet**. These experiments reveal similar rate constants for all of these molecules, spanning from $2.4 \pm 0.2 \times 10^{-3}$ cm s^{-1} (**4-Di**) to $1.1 \pm 0.2 \times 10^{-3}$ cm s^{-1} (**4-Tet**). Self-exchange rates (k_{ex}) for the oligomers were quantified using Nafion-coated electrodes to determine how rapidly the oxidized oligomers redistribute their charge throughout the bulk of uncharged material. The apparent diffusion coefficient was determined for each species at varying concentrations and used in the Dahms–Ruff equation to calculate the self-exchange rate (see Supporting Information for detailed procedures). The self-exchange rate decreases by approximately an order of magnitude per added CP unit, from $7.2 \pm 5.1 \times 10^9$ M^{-1} s^{-1} for **4-Di** to $2.7 \pm 0.2 \times 10^8$ M^{-1} s^{-1} for **4-Tri** and $3.7 \pm 0.2 \times 10^7$ M^{-1} s^{-1} for **4-Tet**. The larger error observed for **4-Di** is attributed to the rapid self-exchange rate, which renders this electron transfer rate more difficult to measure. Overall, a decrease in self-exchange rate with increasing oligomer length is expected, since the backbone/tether is expected to constrain self-exchange. We note that the observed exchange rates for these oligomers remain in the range of well-studied molecules such as ruthenium tris-bipyridine complexes.[35] Additionally, the self-exchange rates for the cyclopropenium oligomers are equal to or higher than those of many monomeric redox-active molecules that have been employed in flow battery applications (e.g., phenothiazine, pentahelicene, and hydroquinone).[35] Collectively, these data show that the CP oligomers undergo facile charge transfer with a carbon electrode as well as between oxidized and reduced CP units in solution. The impressive self-exchange rates also explain the similar bulk electrolysis state-of-charge achieved regardless of oligomer length.

Solubility of the catholyte species is another crucial physical property for NRFB applications, as it is directly linked to the energy density of the battery. The theoretical energy density is defined by the volumetric charge capacity of the anolyte/catholyte pair multiplied by their difference in standard redox potential. For the monomeric cyclopropenium **1**, the maximum charge capacity in acetonitrile is inherently limited by the solubility of the oxidized cyclopropenium $\mathbf{1}^+$.[19] To assess analogous effects with the oligomers, we compared the solubility of $\mathbf{1}^+$ to that of $\mathbf{4\text{-}Di}^{2+}$, $\mathbf{4\text{-}Tri}^{3+}$, and $\mathbf{4\text{-}Tet}^{4+}$. The oxidized compounds were prepared by bulk electrolysis and isolated via precipitation with diethyl ether. The maximum solubility was then quantified in acetonitrile with and without the presence of 0.5 M $LiPF_6$ supporting electrolyte (Figure 4, Table S1). Increasing the number of CP repeat units from one to four results in a decrease in the maximum solubility from 310 to 87 mM in acetonitrile and from 110 to 33 mM in a 0.5 M $LiPF_6$ acetonitrile solution. The nearly 3-fold reduction in solubility when supporting electrolyte is present is expected based on the common ion effect.[36]

Although the overall solubility decreases with a higher number of repeat units, it is important to note that the theoretical maximum charge capacity (8.4 to 10.9 Ah/L in acetonitrile and 2.8 to 4.7 Ah/L in 0.5 M $LiPF_6$ acetonitrile) is nearly identical for all four molecules (monomer, dimer, trimer, and tetramer) due to the concomitant increase in number of transferable electrons per molecule. Next to these solubility data, viscosity measurements of 0.1 M redox equivalent solutions show that there is no significant difference in viscosity

Table 1. Electrochemical Properties and Diffusion Coefficients for CP Oligomers

oligomer	$E_{1/2}$ vs Fc/Fc^+ (V)	D_{sol} CP (cm^2 s^{-1})	D_{sol} oxidized CP (cm^2 s^{-1})	k_0 heterogeneous (cm s^{-1})	k_{ex} self-exchange (M^{-1} s^{-1})	η^a (mPa s^{-1})	D_{eff} PIM-1[b] (cm^2 s^{-1})
1	0.862	$7.0 \pm 0.2 \times 10^{-6}$	$5.9 \pm 0.3 \times 10^{-6}$	$2.2 \pm 0.1 \times 10^{-3}$	nd	0.345 ± 0.009	$5.0 \pm 0.5 \times 10^{-9}$
4-Di	0.867	$2.1 \pm 0.1 \times 10^{-6}$	$1.4 \pm 0.1 \times 10^{-6}$	$2.4 \pm 0.2 \times 10^{-3}$	$7.2 \pm 5.1 \times 10^9$	0.366 ± 0.012	$3.1 \pm 0.4 \times 10^{-10}$
4-Tri	0.865	$1.1 \pm 0.1 \times 10^{-6}$	$4.7 \pm 0.2 \times 10^{-7}$	$1.5 \pm 0.1 \times 10^{-3}$	$2.7 \pm 0.2 \times 10^8$	0.355 ± 0.009	$3.8 \pm 0.5 \times 10^{-11}$
4-Tet	0.860	$5.3 \pm 0.2 \times 10^{-7}$	$2.5 \pm 0.1 \times 10^{-7}$	$1.1 \pm 0.2 \times 10^{-3}$	$3.7 \pm 0.2 \times 10^7$	0.364 ± 0.009	$<2.0 \times 10^{-11}$

[a]Viscosity of 0.1 M redox equivalent oligomer solution in acetonitrile; the viscosity of acetonitrile was determined to be 0.310 mPa s^{-1}. [b]Effective diffusion coefficient of CP oligomer through a cross-linked PIM-1 membrane. The detection limit of the setup was 2.0×10^{-11} cm^2 s^{-1} as determined by the time of the experiment and the lowest detectable concentration of tetramer.

DOI: 10.1021/acscentsci.7b00544
ACS Cent. Sci. 2018, 4, 189–196

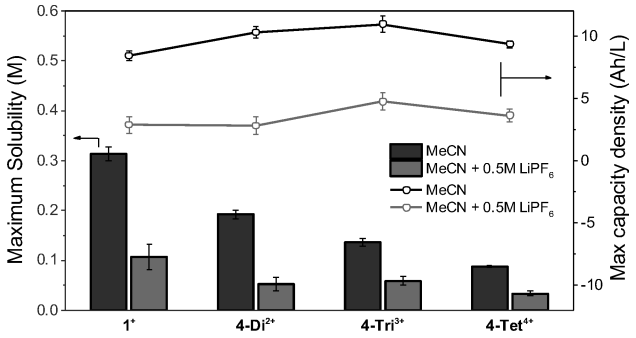

Figure 4. Maximum solubility of oxidized CP oligomers in acetonitrile and 0.5 M $LiPF_6$ acetonitrile, and their corresponding maximum capacity densities.

going from monomer to tetramer (Table 1). Thus, overall, these data demonstrate that the oligomerization strategy imposes no penalty on the maximum achievable volumetric charge capacity or viscosity.

Having demonstrated that the oligomers **4-Di**–**Tet** possess desirable physical properties for a high-performance NRFB catholyte, we next explored their pairing with the microporous PIM-1 membrane. To determine the effect of oligomer length on the rate of diffusion through the PIM-1 membrane, crossover experiments were performed using 8–11 μm thick cross-linked PIM-1 membranes in an H-cell.[29] The permeate was loaded with either 60 mM **1**, 30 mM **4-Di**, 20 mM **4-Tri**, or 15 mM **4-Tet** dissolved in 0.5 M $LiPF_6$ in acetonitrile, and the retentate was loaded with a proportional amount of $LiPF_6$ electrolyte to balance osmotic pressure. Crossover of the CP oligomers was monitored by cyclic voltammetry of the retentate. Figure 5 shows that the monomer **1** rapidly crosses

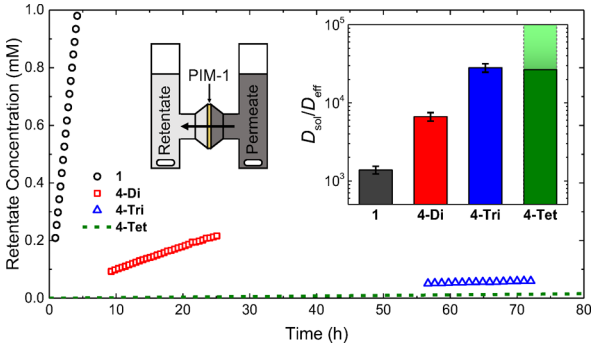

Figure 5. Measured crossover of CP oligomers through a cross-linked PIM-1 membrane using an H-cell; the dashed line indicates the experimental detection limit; left inset shows schematic of the setup. The graph inset shows the calculated effective diffusion coefficients corrected for diffusion in solution; the value for **4-Tet** is estimated from the detection limit of the setup and represents a lower bound for D_{sol}/D_{eff}.

through the membrane with an effective diffusion coefficient (D_{eff}) of 5.0 ± 0.5 × 10^{-9} cm^2 s^{-1}. For **4-Di** and **4-Tri**, the diffusion coefficient decreases to 3.1 ± 0.4 × 10^{-10} and 3.8 ± 0.5 × 10^{-11} cm^2 s^{-1}, respectively. Finally, no crossover of **4-Tet** was detected over the course of the experiment (192 h), indicating highly effective size-sieving by the PIM-1 membrane. Correcting the effective diffusion coefficients through the PIM-1 membrane for the diffusion coefficients of the molecules in solution (D_{sol}, determined from the CV experiments; Table 1) demonstrates the same trend. D_{sol}/D_{eff} reveals a 4- to 5-fold enhancement in separating ability per added CP repeating unit (Figure 5, inset). As such, diffusion of the tetramer through the PIM-1 membrane is approximately ∼100,000 times slower than diffusion in solution, resulting in highly effective size exclusion.

We next transitioned from fundamental studies to a proof-of-concept demonstration, pairing the optimal oligomer, **4-Tet**, with a PIM-1 membrane in a redox flow battery. As shown in Figure 6a, our redox flow battery is composed of graphite charge collecting plates with an interdigitated flow field, in combination with 400 μm thick carbon-felt electrodes.[37,38] The membrane separating the two half-cells is a cross-linked PIM-1 membrane (∼15 μm thickness), sandwiched between two layers of Celgard 2500 for mechanical support.[39] Notably, the two layers of Celgard contribute only a nominal 3 Ω cm^2 resistance to the overall area specific resistance (ASR) of the membrane stack in these systems (overall ASR = 21–26 Ω cm^2, see Figure S4b).

A solution of 12.5 mM **4-Tet** in acetonitrile was used as the catholyte (6 mL). Because a stable oligomeric anolyte has yet to be identified, a 2-fold redox equivalent excess (100 mM, 6 mL) of monomeric 4-benzoyl-1-isopropylpyridinium was used as the anolyte ($E_{1/2}$ = −1.05 V vs Fc/Fc^+).[18] KPF_6 (0.5 M) was selected as the supporting electrolyte to facilitate stable cycling of both anolyte and catholyte.[40] Overall, this yields a battery with an open-circuit voltage of 1.9 V and a theoretical energy density of 1.3 Wh/L. The monomeric anolyte is expected to diffuse through the PIM-1 membrane over the course of the experiment, ultimately leading to a reduction of the charge capacity when sufficient anolyte has crossed over. However, the added excess should enable initial monitoring of catholyte cycling performance in flow, while allowing for detection of catholyte crossover after the experiment.[41]

The battery was galvanostatically cycled using a charging current of 2.5 mA/cm^2 and a discharge current of 5 mA/cm^2 with a flow rate of 10 mL/min, achieving a 96% SOC at this rate. Figure 6b displays the discharge capacity vs cycle number and demonstrates good capacity retention through the first 17 cycles (<5% loss), with an average Coulombic efficiency of 95% and an energy efficiency of 79% (Figure 6c). After these cycles, the anticipated crossover of the monomeric pyridinium anolyte resulted in the anolyte concentration dropping below 1 equiv relative to the catholyte, ultimately accelerating capacity fade. These results are consistent with cyclic voltammetry analysis of the anolyte and catholyte before and after the 2 days of battery cycling, which show crossover of the pyridinium anolyte into the catholyte reservoir, but no detectable crossover of the tetrameric catholyte into the anolyte reservoir (Figure 6d, Figure S4e). No crossover of the catholyte was detected even after allowing the solutions to flow through the setup for a total of 6 days, emphasizing the highly effective separation imparted by this membrane stack (Figure S4d).

A key advantage of developing oligomers based on well-studied parent monomers is the opportunity to directly compare the performance of the two species. Thus, the cyclopropenium monomer was subjected to an identical cycling study using 50 mM **1** as the catholyte. As anticipated, the monomer experienced a significantly faster capacity fade, owing to rapid and deleterious crossover of the monomer (Figure 6b, 13% fade within 15 cycles). Cyclic voltammetry at the end of this battery cycling experiment clearly showed the presence of monomer **1** in the anolyte solution (Figure 6d). These results are fully consistent with the crossover studies conducted in the

DOI: 10.1021/acscentsci.7b00544
ACS Cent. Sci. 2018, 4, 189–196

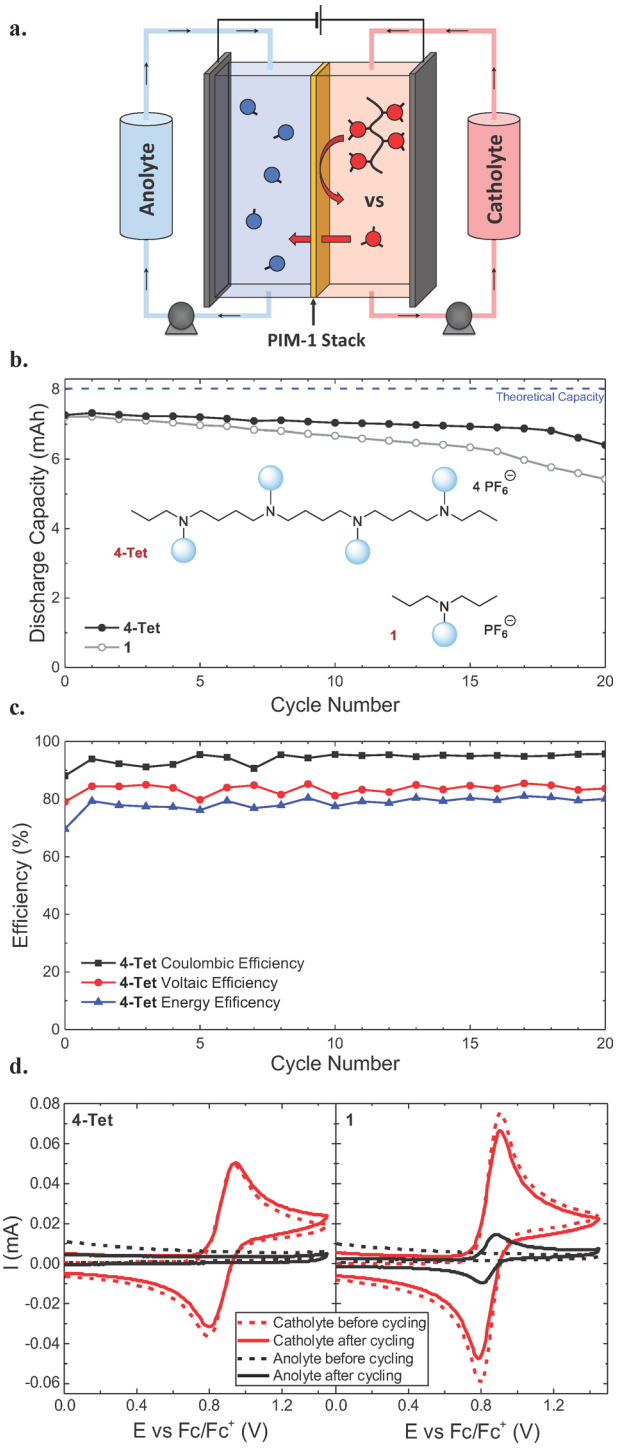

Figure 6. (a) Schematic overview of the proof-of-concept redox flow battery. (b) Discharge capacity vs cycle number of the redox flow battery using 12.5 mM **4-Tet** and 50 mM **1**. (c) Coulombic, voltaic, and energy efficiencies of cycling experiment using **4-Tet**. (d) Cyclic voltammograms at 100 mV s^{-1} of flow battery electrolyte aliquots of **1** and **4-Tet** before and after the cycling experiments.

static H-cell (Figure 5). Overall, these proof-of-concept batteries demonstrate the feasibility of combining an oligomeric redox-active material with a microporous membrane for an NRFB.

In summary, this article describes the development of a stable, high potential oligomeric catholyte that is designed to be paired with a microporous size-exclusion membrane for use in nonaqueous redox flow batteries. Initial evaluation of a series of dimeric derivatives revealed that an *n*-butyl spacer is required between the redox-active moieties in order to achieve electrochemical stability. A series of *n*-butyl-linked oligomers was then prepared, and studies revealed that increasing the oligomer size from monomer to tetramer imposed no penalty on the theoretical charge capacity, while coinciding with only a small reduction in the solution diffusion and electron self-exchange rates. Furthermore, the tetramer displayed no measurable crossover through a cross-linked PIM-1 membrane. Finally, the tetramer was deployed in a proof-of-concept flow battery and cycled successfully for over 2 days. Importantly, no crossover of the tetramer was observed during this time, nor when flowing the electrolyte solutions for a total of 6 days. Our ongoing efforts are focused on identifying electrochemically stable oligomeric anolytes that are effectively excluded by PIM-1 membranes to be paired with the CP tetramer presented here. Additionally, the development of CP oligomers with increased solubility in acetonitrile/$LiPF_6$ is underway, in order to ultimately achieve enhanced energy densities in these systems. Finally, ongoing efforts are directed at decreasing the thickness of the PIM-1 membrane while maintaining structural integrity, in order to reduce the ASR and allow for higher current densities. Overall, these efforts will enable the realization of a high energy density asymmetric oligomer-based NRFB.

■ ASSOCIATED CONTENT

Supporting Information

The Supporting Information is available free of charge on the ACS Publications website at DOI: 10.1021/acscentsci.7b00544.

Synthesis, purification, and characterization of reported compounds, and detailed procedures and additional figures on electrochemical methods, self-exchange studies, and crossover studies (PDF)

■ AUTHOR INFORMATION

Corresponding Author

*E-mail: mssanfor@umich.edu.

ORCID

Brett A. Helms: 0000-0003-3925-4174
Matthew S. Sigman: 0000-0002-5746-8830
Shelley D. Minteer: 0000-0002-5788-2249
Melanie S. Sanford: 0000-0001-9342-9436

Notes

The authors declare no competing financial interest.

■ ACKNOWLEDGMENTS

This research was supported by the Joint Center for Energy Storage Research (JCESR), a U.S. Department of Energy, Energy Innovation Hub. S.G.R acknowledges the NSF for a graduate research fellowship. Portions of this work, including polymer synthesis and characterization, membrane preparation, and crossover measurements, were carried out as a user project at the Molecular Foundry, which is supported by the Office of Science, Office of Basic Energy Sciences of the U.S. Department of Energy under Contract No. DE-AC02-05CH11231.

DOI: 10.1021/acscentsci.7b00544
ACS Cent. Sci. 2018, 4, 189−196

REFERENCES

(1) Soloveichik, G. L. Flow batteries: current status and trends. *Chem. Rev.* **2015**, *115*, 11533−11558.
(2) Winsberg, J.; Hagemann, T.; Janoschka, T.; Hager, M. D.; Schubert, U. S. Redox-flow batteries: from metals to organic redox-active materials. *Angew. Chem., Int. Ed.* **2017**, *56*, 686−711.
(3) Kamat, P. V.; Schanze, K. S.; Buriak, J. M. Redox Flow Batteries. *ACS Energy Lett.* **2017**, *2*, 1368−1369.
(4) Wei, X. L.; Duan, W. T.; Huang, J. H.; Zhang, L.; Li, B.; Reed, D.; Xu, W.; Sprenkle, V.; Wang, W. A high-current, stable nonaqueous organic redox flow battery. *ACS Energy Lett.* **2016**, *1*, 705−711.
(5) Milshtein, J. D.; Kaur, A. P.; Casselman, M. D.; Kowalski, J. A.; Modekrutti, S.; Zhang, P. L.; Attanayake, N. H.; Elliott, C. F.; Parkin, S. R.; Risko, C.; Brushett, F. R.; Odom, S. A. High current density, long duration cycling of soluble organic active species for non-aqueous redox flow batteries. *Energy Environ. Sci.* **2016**, *9*, 3531−3543.
(6) Leung, P.; Shah, A. A.; Sanz, L.; Flox, C.; Morante, J. R.; Xu, Q.; Mohamed, M. R.; Ponce de León, C.; Walsh, F. C. Recent developments in organic redox flow batteries: a critical review. *J. Power Sources* **2017**, *360*, 243−283.
(7) Ding, Y.; Zhao, Y.; Li, Y.; Goodenough, J. B.; Yu, G. A high-performance all-metallocene-based, non-aqueous redox flow battery. *Energy Environ. Sci.* **2017**, *10*, 491−497.
(8) Noack, J.; Roznyatovskaya, N.; Herr, T.; Fischer, P. The chemistry of redox-flow batteries. *Angew. Chem., Int. Ed.* **2015**, *54*, 9776−9809.
(9) Beh, E. S.; De Porcellinis, D.; Gracia, R. L.; Xia, K. T.; Gordon, R. G.; Aziz, M. J. A neutral pH aqueous organic/organometallic redox flow battery with extremely high capacity retention. *ACS Energy Lett.* **2017**, *2*, 639−644.
(10) Perry, M. L.; Weber, A. Z. Advanced redox-flow batteries: A perspective. *J. Electrochem. Soc.* **2016**, *163*, A5064−A5067.
(11) Huskinson, B.; Marshak, M. P.; Suh, C.; Er, S.; Gerhardt, M. R.; Galvin, C. J.; Chen, X.; Aspuru-Guzik, A.; Gordon, R. G.; Aziz, M. J. A metal-free organic−inorganic aqueous flow battery. *Nature* **2014**, *505*, 195−198.
(12) Lin, K.; Gómez-Bombarelli, R.; Beh, E. S.; Tong, L.; Chen, Q.; Valle, A.; Aspuru-Guzik, A.; Aziz, M. J.; Gordon, R. G. A redox-flow battery with an alloxazine-based organic electrolyte. *Nature Energy* **2016**, *1*, 16102.
(13) Janoschka, T.; Martin, N.; Hager, M. D.; Schubert, U. S. An aqueous redox-flow battery with high capacity and power: the TEMPTMA/MV system. *Angew. Chem., Int. Ed.* **2016**, *55*, 14427−14430.
(14) Hu, B.; DeBruler, C.; Rhodes, Z.; Liu, T. L. Long-cycling aqueous organic redox flow battery (AORFB) toward sustainable and safe energy storage. *J. Am. Chem. Soc.* **2017**, *139*, 1207−1214.
(15) Kear, G.; Shah, A. A.; Walsh, F. C. Development of the all-vanadium redox flow battery for energy storage: a review of technological, financial and policy aspects. *Int. J. Energy Res.* **2012**, *36*, 1105−1120.
(16) Wang, W.; Sprenkle, V. Redox flow batteries go organic. *Nat. Chem.* **2016**, *8*, 204−206.
(17) Schon, T. B.; McAllister, B. T.; Li, P. F.; Seferos, D. S. The rise of organic electrode materials for energy storage. *Chem. Soc. Rev.* **2016**, *45*, 6345−6404.
(18) Sevov, C. S.; Hickey, D. P.; Cook, M. E.; Robinson, S. G.; Barnett, S.; Minteer, S. D.; Sigman, M. S.; Sanford, M. S. Physical organic approach to persistent, cyclable, low-potential electrolytes for flow battery applications. *J. Am. Chem. Soc.* **2017**, *139*, 2924−2927.
(19) Sevov, C. S.; Samaroo, S. K.; Sanford, M. S. Cyclopropenium salts as cyclable, high-potential catholytes in nonaqueous media. *Adv. Energy Mater.* **2017**, *7*, 1602027.
(20) Zhang, J.; Yang, Z.; Shkrob, I. A.; Assary, R. S.; Tung, S.; Silcox, B.; Duan, W.; Zhang, J.; Su, C. C.; Hu, B.; Pan, B.; Liao, C.; Zhang, Z.; Wang, W.; Curtiss, L. A.; Thompson, L. T.; Wei, X.; Zhang, L. Annulated dialkoxybenzenes as catholyte materials for non-aqueous redox flow batteries: achieving high chemical stability through bicyclic substitution. *Adv. Energy Mater.* **2017**, *7*, 1701272.
(21) Shin, S.-H.; Yun, S.-H.; Moon, S.-H. A review of current developments in non-aqueous redox flow batteries: characterization of their membranes for design perspective. *RSC Adv.* **2013**, *3*, 9095−9116.
(22) Wang, W.; Luo, Q. T.; Li, B.; Wei, X. L.; Li, L. Y.; Yang, Z. G. Recent progress in redox flow battery research and development. *Adv. Funct. Mater.* **2013**, *23*, 970−986.
(23) Janoschka, T.; Martin, N.; Martin, U.; Friebe, C.; Morgenstern, S.; Hiller, H.; Hager, M. D.; Schubert, U. S. An aqueous, polymer-based redox-flow battery using non-corrosive, safe, and low-cost materials. *Nature* **2015**, *527*, 78−81.
(24) Nagarjuna, G.; Hui, J.; Cheng, K. J.; Lichtenstein, T.; Shen, M.; Moore, J. S.; Rodríguez-López, J. Impact of redox-active polymer molecular weight on the electrochemical properties and transport across porous separators in nonaqueous solvents. *J. Am. Chem. Soc.* **2014**, *136*, 16309−16316.
(25) Burgess, M.; Moore, J. S.; Rodríguez-López, J. Redox active polymers as soluble nanomaterials for energy storage. *Acc. Chem. Res.* **2016**, *49*, 2649−2657.
(26) Montoto, E. C.; Nagarjuna, G.; Moore, J. S.; Rodríguez-López, J. Redox active polymers for non-aqueous redox flow batteries: validation of the size-exclusion approach. *J. Electrochem. Soc.* **2017**, *164*, A1688−A1694.
(27) Winsberg, J.; Hagemann, T.; Muench, S.; Friebe, C.; Häupler, B.; Janoschka, T.; Morgenstern, S.; Hager, M. D.; Schubert, U. S. Poly(boron-dipyrromethene) A redox-active polymer class for polymer redox-flow batteries. *Chem. Mater.* **2016**, *28*, 3401−3405.
(28) Burgess, M.; Chénard, E.; Hernández-Burgos, K.; Nagarjuna, G.; Assary, R. S.; Hui, J.; Moore, J. S.; Rodríguez-López, J. Impact of backbone tether length and structure on the electrochemical performance of viologen redox active polymers. *Chem. Mater.* **2016**, *28*, 7362−7374.
(29) Doris, S. E.; Ward, A. L.; Baskin, A.; Frischmann, P. D.; Gavvalapalli, N.; Chénard, E.; Sevov, C. S.; Prendergast, D.; Moore, J. S.; Helms, B. A. Macromolecular design strategies for preventing active-material crossover in non-aqueous all-organic redox-flow batteries. *Angew. Chem., Int. Ed.* **2017**, *56*, 1595−1599.
(30) Budd, P. M.; Ghanem, B. S.; Makhseed, S.; McKeown, N. B.; Msayib, K. J.; Tattershall, C. E. Polymers of intrinsic microporosity (PIMs): Robust, solution-processable, organic nanoporous materials. *Chem. Commun.* **2004**, 230−231.
(31) Dmello, R.; Milshtein, J. D.; Brushett, F. R.; Smith, K. C. Cost-driven materials selection criteria for redox flow battery electrolytes. *J. Power Sources* **2016**, *330*, 261−272.
(32) Darling, R. M.; Gallagher, K. G.; Kowalski, J. A.; Ha, S.; Brushett, F. R. Pathways to low-cost electrochemical energy storage: a comparison of aqueous and nonaqueous flow batteries. *Energy Environ. Sci.* **2014**, *7*, 3459−3477.
(33) See ref 19 for a discussion of possible decomposition pathways for oxidized CP molecules.
(34) Weber, A. Z.; Mench, M. M.; Meyers, J. P.; Ross, P. N.; Gostick, J. T.; Liu, Q. Redox flow batteries: a review. *J. Appl. Electrochem.* **2011**, *41*, 1137−1164.
(35) Eberson, L. *Electron-transfer reactions in organic chemistry*; Academic Press: London, 1982; Vol. *18*.
(36) Shin, E. S.; Kim, K.; Oh, S. H.; Cho, W. I. Polysulfide dissolution control: the common ion effect. *Chem. Commun.* **2013**, *49*, 2004−2006.
(37) Milshtein, J. D.; Kaur, A. P.; Casselman, M. D.; Kowalski, J. A.; Modekrutti, S.; Zhang, P. L.; Harsha Attanayake, N.; Elliott, C. F.; Parkin, S. R.; Risko, C.; Brushett, F. R.; Odom, S. A. High current density, long duration cycling of soluble organic active species for non-aqueous redox flow batteries. *Energy Environ. Sci.* **2016**, *9*, 3531−3543.
(38) Milshtein, J. D.; Barton, J. L.; Darling, R. M.; Brushett, F. R. 4-acetamido-2,2,6,6-tetramethylpiperidine-1-oxyl as a model organic redox active compound for nonaqueous flow batteries. *J. Power Sources* **2016**, *327*, 151−159.
(39) Initial attempts at battery operation revealed that the use of a cross-linked PIM-1 membrane on its own resulted in rapid mechanical

DOI: 10.1021/acscentsci.7b00544
ACS Cent. Sci. 2018, 4, 189−196

failure of the membrane. However, sandwiching the microporous membrane between two layers of Celgard 2500 provided sufficient mechanical support to enable flow cell operation.

(40) Hendriks, K. H.; Sevov, C. S.; Cook, M. E.; Sanford, M. S. Multielectron Cycling of a low-potential anolyte in alkali metal electrolytes for nonaqueous redox flow batteries. *ACS Energy Lett.* **2017**, *2*, 2430−2435.

(41) Crossover of reduced anolyte is expected to cause a small reduction of the Coulombic efficiency. Otherwise, the two redox compounds do not interfere with each other's redox chemistry when mixed (Figure S4c).

DOI: 10.1021/acscentsci.7b00544
ACS Cent. Sci. 2018, 4, 189−196